

Competition for light color between marine *Synechococcus* strains with fixed and variable pigmentation

Louison Dufour,¹ Laurence Garczarek,¹ Francesco Mattei,² Bastian Gouriou,¹ Julia Clairet,¹ Morgane Ratin,¹ David M. Kehoe,³ Jef Huisman,⁴ Jolanda M. H. Verspagen,⁴ Frédéric Partensky¹

AUTHOR AFFILIATIONS See affiliation list on p. 18.

ABSTRACT Competition between phytoplankton species for light has triggered extensive diversification of photosynthetic pigments. In *Synechococcus* cyanobacteria, three major pigment types occur in the ocean: blue light (BL) specialists that have a high ratio of the BL-absorbing chromophore phycourobilin (PUB) to the green light (GL)-absorbing chromophore phycoerythrobilin (PEB), GL specialists that have a low PUB:PEB ratio, and cells that modify their PUB:PEB ratio to match the ambient color, a process called "Type IV chromatic acclimation" (CA4). The abundance of CA4-capable cells in marine ecosystems suggests that CA4 confers a fitness advantage in certain light conditions compared to cells with fixed pigmentation. This hypothesis was tested by performing mono- and co-cultures of a BL specialist, a GL specialist, and a CA4-capable strain in chemostats under different light conditions. Monocultures enabled us to parameterize a resource competition model that was used to predict competition between the three pigment types in co-cultures. In line with the model predictions, the BL specialist won in low blue light and the GL specialist won in low and high green light. Interestingly, we found that while the CA4-capable strain was at a disadvantage at low light, it was able to outcompete specialists in high blue light.

IMPORTANCE *Synechococcus* cyanobacteria are ubiquitous and abundant in the lit layer of most marine ecosystems. This ubiquity relies in part on the wide pigment diversity of their light-harvesting complexes, with three main pigment types thriving in open ocean waters: green light specialists, blue light specialists, and chromatic acclimators, the latter being capable of matching their pigment content to the ambient spectral field. Here, we simulated the competition for light color that occurs between these pigment types in the field by co-culturing them in various light color and intensity conditions, and compared the resulting data to that of a competition model. This study provides new insights into how this key group of phytoplankton colonizes the various spectral niches of the marine environment.

KEYWORDS marine picocyanobacteria, *Synechococcus*, pigment type, chromatic acclimation, competition model

Although marine phytoplankton accounts for approximately half of global net primary production, their contribution is highly variable spatially, depending on community composition, which is greatly influenced by local environmental conditions (1, 2). Despite their apparent continuity, the world's oceans indeed encompass many different ecological niches delineated by temperature gradients and changes in the relative availability of two types of essential resources for which phytoplankton taxa compete: light and nutrients. Light, which provides the energy required for photosynthesis, fluctuates both quantitatively and qualitatively in the water column. The exponential decrease in light irradiance with depth is accompanied by a progressive narrowing

Editor Julia C. van Kessel, Indiana University
Bloomington, Bloomington, Indiana, USA

Address correspondence to Frédéric Partensky,
frederic.partensky@sb-roscoff.fr.

The authors declare no conflict of interest.

See the funding table on p. 19.

Ed. Note: A potential conflict of interest was identified after acceptance of this paper, and the Editor in Chief performed an additional final review of the paper.

Received 13 January 2025

Accepted 4 June 2025

Published 24 July 2025

Copyright © 2025 Dufour et al. This is an open-access article distributed under the terms of the [Creative Commons Attribution 4.0 International license](https://creativecommons.org/licenses/by/4.0/).

of the visible light spectrum because of the absorption of different wavelengths by water, dissolved organic matter, particles, and phytoplankton. The spectral field also strongly varies horizontally from coastal particle-rich to clear open ocean waters (3, 4). In this context, Holtrop et al. (5) recently defined five distinct spectral niches in aquatic ecosystems (violet, blue, green, orange, and red niches), with the last two being restricted to freshwater, estuaries, and near-coastal environments. Competition for light occurring in these five niches has triggered a wide diversification of photosynthetic pigments used to collect photosynthetically active radiation (PAR) and photoprotective pigments, the latter being needed to cope with strong irradiances occurring in the upper euphotic layer. This pigment variability allows different phytoplankton taxa to coexist by spectral niche differentiation, that is, by collecting distinct parts of the visible light spectrum (6, 7).

A striking example of this pigment diversification can be seen in marine *Synechococcus*. With an estimated global abundance of 7×10^{26} cells, this ubiquitous picocyanobacterium is the second-most abundant organism in the world's oceans (8) and exhibits the largest pigment diversity within a single phytoplankton lineage known so far (9–11). Like most other cyanobacteria, *Synechococcus* uses large, hydrophilic light-harvesting complexes called phycobilisomes (PBS) to collect photons and transfer their energy to photosystems (PS) I and II (12, 13). *Synechococcus* PBS are composed of a core from which extend six to eight peripheral rods (14, 15). Both core and rods are made of α - β heterodimers of phycobiliproteins assembled into $(\alpha\text{-}\beta)_6$ hexamers held together by linker proteins. While the PBS core is predominantly composed of allophycocyanin (APC, maximum absorption wavelength $\lambda_{\text{max}} \approx 650$ nm), rods can be made of either phycocyanin (PC, $\lambda_{\text{max}} \approx 620$ nm) or a combination of PC and one or two additional types of phycoerythrin (PE-I and PE-II, $\lambda_{\text{max}} \approx 560$ nm [9, 13]). Each phycobiliprotein α - β heterodimer covalently binds between two (in APC) and six (in PE-II) chromophores at the level of highly conserved cysteine residues, an attachment generally catalyzed by phycobilin lyases (16). In marine *Synechococcus*, three distinct types of chromophores have been reported: phycocyanobilin (PCB, $\lambda_{\text{max}} \approx 630$ nm), phycoerythrobilin (PEB, $\lambda_{\text{max}} \approx 550$ nm), and phycourobilin (PUB, $\lambda_{\text{max}} \approx 495$ nm [14]).

Three main pigment types (PTs) have been defined among *Synechococcus* strains based on the phycobiliprotein composition of PBS rods, with PT 1 possessing only PC, PT 2 containing both PC and PE-I, and PT 3 having PC, PE-I, and PE-II. PT 3 was further divided into subtypes based on the relative cell content of PUB and PEB, as estimated by the relative ratio of fluorescence excitation at 495 and 550 nm ($\text{Exc}_{495:550}$), with emission set at 580 nm. More precisely, the PUB:PEB ratio is low ($\text{Exc}_{495:550} < 0.5$) in subtype 3a, high ($\text{Exc}_{495:550} \geq 1.6$) in subtype 3c, and variable in subtype 3d (9, 10). The pigmentation of PT 3a and 3c strains remains fixed in changing light qualities, so they are often referred to as “green light (GL) specialists” and “blue light (BL) specialists,” respectively (17). By contrast, PT 3d strains are capable of reversibly modifying their $\text{Exc}_{495:550}$ ratio from 0.6–0.7 in GL to 1.6–1.7 in BL, a process called “Type IV chromatic acclimation” (hereafter CA4 [18–20]). Two genetically distinct types of CA4-capable strains (PTs 3dA and 3dB) have been described (10, 21), each possessing a small genomic island specifically involved in this process, and called the “CA4-A” or “CA4-B” island, respectively. Interestingly, it has been suggested that during evolution, the acquisition of the CA4-A island conferred the ability to chromatically acclimate to GL specialists, and conversely, that the CA4-B island provided the same ability to BL specialists (22–25).

The ecological significance of the CA4 process has long remained elusive due to the lack of an effective method to discriminate CA4-capable strains from BL and GL specialists. However, using three different PBS gene markers, Grébert and co-workers (26) were able to quantify the relative abundances of the different *Synechococcus* PTs throughout much of the world's oceans using metagenomic data from the Tara Oceans expedition. These authors demonstrated that CA4-capable cells accounted for ca. 41.5% of the total marine *Synechococcus* population, with PT 3dA and 3dB cells being almost equally abundant (22.6% and 18.9%, respectively) but colonizing complementary

TABLE 1 Characteristics of the three *Synechococcus* strains used in this study

Characteristic	Value for strain:		
	RS9902	RS9907	RS9915
RCC ^a number	2676	2382	2553
Subcluster ^b	5.1	5.1	5.1
Clade ^b	II	II	III
Subclade ^c	Ila	Ila	IIla
Pigment type ^d	3c (BL specialist)	3a (GL specialist)	3dB (CA4-capable)
Isolation date ^b	1999-03-29	1999-08-23	1999-10-18

^aRoscoff Culture Collection.^bReference 29.^cReference 30.^dReference 10.

ecological niches in the field. PT 3dA cells dominated in temperate and high-latitude waters, while PT 3dB cells were more abundant in warm tropical waters. By comparison, the GL and BL specialists were found to represent 20.3% and 33.4% of the global *Synechococcus* population, respectively. The GL specialists were shown to be more abundant in near-coastal particle-rich waters where green light predominates, while the BL specialists prevailed in clear open ocean waters where blue wavelengths dominate the underwater light field (5, 26, 27). The prevalence of CA4-capable strains in marine ecosystems suggests that, in some light conditions, CA4 may confer a fitness advantage to cells that allows them to co-occur with, and even sometimes outcompete, cells with fixed pigmentation.

To test this hypothesis, we performed continuous mono- and co-cultures of a BL specialist, a GL specialist, and a CA4-capable strain (belonging to PT 3dB), all coming from the same location in the Red Sea (Table 1). These experiments were performed in chemostats (28) under different conditions of light quantity (15 and 75 $\mu\text{mol photons m}^{-2} \text{s}^{-1}$) and quality (BL and GL). In addition, a series of photo-physiological measurements were carried out on all strains to determine their respective adaptive value and better understand the outcomes of competition experiments. Monocultures enabled us to parameterize a resource competition model, which was subsequently used to investigate competition for light between the three *Synechococcus* strains. The theoretical predictions were afterward confirmed by conducting co-cultures with all three representatives. Altogether, we demonstrated that while the CA4-capable strain was at a disadvantage at low light, it was able to outcompete cells with fixed pigmentation in high blue light.

Competition model

The resource competition model describes competition for light of different colors among phytoplankton species with different pigments. The model extends earlier competition models by Stomp and colleagues (6, 27) and was previously described (31). The model assumes a well-mixed water column that is illuminated from above with an incident light spectrum, $I(\lambda)$, where λ represents wavelength. The underwater light spectrum $I(\lambda, z)$ changes qualitatively with water depth z due to absorption of different wavelengths by phytoplankton, water, dissolved organic matter ("gilvin"), and suspended particles ("tripton"). At each wavelength, light intensity diminishes exponentially with depth according to Lambert-Beer's law, so that the underwater light spectrum over depth can be represented as:

$$I(\lambda, z) = I_{\text{in}}(\lambda) \exp\left(-\sum_{i=1}^n k_i(\lambda) C_i z - K_{\text{bg}}(\lambda) z\right) \quad (\text{Eq. 1})$$

Here, $k_i(\lambda)$ represents the absorption spectrum of phytoplankton species i , and C_i is the population density of species i . The summation term signifies light absorption by n different phytoplankton species, each having its distinct absorption spectrum.

The absorption of photons by water, gilvin, and tripton is incorporated in the wavelength-specific background turbidity $K_{bg}(\lambda)$. Furthermore, $I_{out}(\lambda)$ is defined as the light spectrum at the bottom of the water column, so that $I_{out}(\lambda) = I(\lambda, z_m)$, where z_m is the water column depth.

The population density of each phytoplankton species i changes dynamically through growth and loss processes:

$$\frac{dC_i}{dt} = \left(\frac{1}{z_m} \int_0^{z_m} \int_{400}^{700} p_i(\lambda, z) d\lambda dz - m_i \right) C_i \quad (\text{Eq. 2})$$

where we have $i = 1, \dots, n$ different species in the community, $p_i(\lambda, z)$ is the specific production rate of species i as a function of wavelength λ and depth z , and m_i is the specific loss rate of species i . Since our experiments were performed at relatively low, non-saturating light intensities, we here assume that the specific production rate depends linearly on the quantity of photons absorbed by species i and the efficiency with which these photons are used:

$$p_i(\lambda, z) = \phi_i(\lambda) k_i(\lambda) I(\lambda, z) \quad (\text{Eq. 3})$$

where $\phi_i(\lambda)$ is the photosynthetic efficiency, that is, the efficiency with which species i converts absorbed photons into the production of biomass. The photosynthetic efficiency may vary with wavelength (31).

With some algebra, the depth integral in equation 2 can be solved with the help of equation 1 and equation 3. We then obtain:

$$\frac{dC_i}{dt} = \left(\int_{400}^{700} \phi_i(\lambda) k_i(\lambda) I_{avg}(\lambda) d\lambda - m_i \right) C_i \quad (\text{Eq. 4})$$

where the depth-averaged light intensity in the water column, $I_{avg}(\lambda)$, is defined as:

$$\begin{aligned} I_{avg}(\lambda) &= \frac{1}{z_m} \int_0^{z_m} I(\lambda, z) dz \\ &= \frac{I_{in}(\lambda) - I_{out}(\lambda)}{\ln(I_{in}(\lambda)) - \ln(I_{out}(\lambda))} \end{aligned} \quad (\text{Eq. 5})$$

In our experiments, we used only two colors, BL and GL, rather than the full light spectrum. In this case, the population dynamics in equation 4 can be simplified to:

$$\frac{dC_i}{dt} = (\phi_i(BL) k_i(BL) I_{avg}(BL) + \phi_i(GL) k_i(GL) I_{avg}(GL) - m_i) C_i \quad (\text{Eq. 6})$$

where the specific production rate is summed over the two colors BL and GL to obtain the total growth rate of species i .

According to this competition model, the species interacts with each other by their modification of the underwater light spectrum. That is, if the population density of a species increases, then it diminishes the intensity and alters the spectral composition of light (via equation 1). These changes in the underwater light field, in turn, affect the population dynamics of itself and the other species in the community (via equations 5 and 6).

MATERIALS AND METHODS

Biological material and culture conditions

Three *Synechococcus* strains, a GL specialist (RS9907, PT 3a), a BL specialist (RS9902, PT 3c), and a CA4-capable strain (RS9915, PT 3dB; Table 1) were obtained from the Roscoff Culture Collection (<https://roscoff-culture-collection.org/>). All were isolated from the upper mixed layer at Station A in the Gulf of Aqaba (Red Sea) in 1999, but at different seasons (29). Cells were grown in PCR-S11 medium (32) supplemented with 175 μM $\text{K}_2\text{HPO}_4 \cdot 3\text{H}_2\text{O}$, and 2 mM NaNO_3 . Before starting the experiments, cultures were pre-acclimated for at least 1 month in temperature-controlled chambers at 25°C to the four different light conditions tested in this study: low blue light (LBL), low green light (LGL), high blue light (HBL), and high green light (HGL). Low (LL) and high light (HL) conditions corresponded, respectively, to 15 and 75 $\mu\text{mol photons m}^{-2} \text{ s}^{-1}$. Continuous light was provided by blue and/or green LEDs (Alpheus). Spectra of incident light and maximum emission wavelengths ($\lambda_{\text{maxBL}} = 475 \text{ nm}$ and $\lambda_{\text{maxGL}} = 515 \text{ nm}$) are provided in Fig. S1. It should be noted that the green LEDs used in this study peaked in the valley between the PUB and PEB excitation peaks. Yet, in a separate study (21), we found that when acclimated to these green LEDs, all tested CA4-capable strains (including RS9915) exhibited the minimal $\text{Exc}_{495:550}$ ratio expected for such CA4-capable cells, demonstrating that they sensed this light color as being “pure GL.”

For each light condition, continuous mono- and co-cultures of the three *Synechococcus* PTs were grown in chemostats (28) inoculated at an initial cell density of 3×10^6 cells mL^{-1} of each strain, so that co-cultures started with an initial concentration of 9×10^6 cells mL^{-1} . Cells were grown in Pyrex Roux flasks (SCI Labware) and continuously diluted until the culture reached the steady state, that is, at least five consecutive days with less than 10% variation in cell density (33). Each flask was equipped with a five-inlet silicone cap for (i) passive ventilation through a 0.2 μm air filter (Midisart 2000, Sartorius), (ii) continuous supply (41.7 $\mu\text{L min}^{-1}$, corresponding to a dilution rate of 0.1 day^{-1}) of PCR-S11 medium using peristaltic pumps (Ismatec Reglo ICC, Cole-Parmer), (iii) continuous removal of the overflow so that the volume in flasks remained constant over time, (iv) aeration with 3% CO_2 -enriched air to control the pH of the cultures and avoid carbon deficiencies, and (v) sample collection (Fig. 1). Because chemostat experiments are demanding, many previous competition studies in chemostats lacked replication (6, 31, 33). However, to increase confidence in the results, our chemostat experiments were done in biological duplicates, unless specified otherwise.

For each mono- and co-culture, samples were harvested every 1 or 2 days to measure cell concentration, PSII quantum yield, chromophore and phycobiliprotein ratios, light intensity, and pH. In addition, 5 mL aliquots from each of the co-cultures were collected at the same frequency, filtered through 0.2 μm Supor filters (Pall Life Sciences), and kept at -80°C until analysis by real-time quantitative PCR.

Flow cytometry

Culture aliquots were sampled every day, fixed with 0.25% (vol/vol) glutaraldehyde (grade II, Sigma Aldrich), and stored at -80°C until analysis. *Synechococcus* cell densities were determined as previously described (34) using a Guava easyCyte flow cytometer equipped with a 488 nm laser and the Guavasoft software (Luminex Corporation).

PAR measurements

Before starting the experiments, the integrated intensity (over 400–700 nm) of the incident light (I_{in}), as well as the light transmitted through the culture flasks (I_{out}) filled with fresh PCR-S11 medium only, were measured with a PG200N Spectral PAR Meter (UPRtek) at five different locations at the surface of flasks, and the values averaged. During the experiments, (I_{out}) was measured daily in the same way.

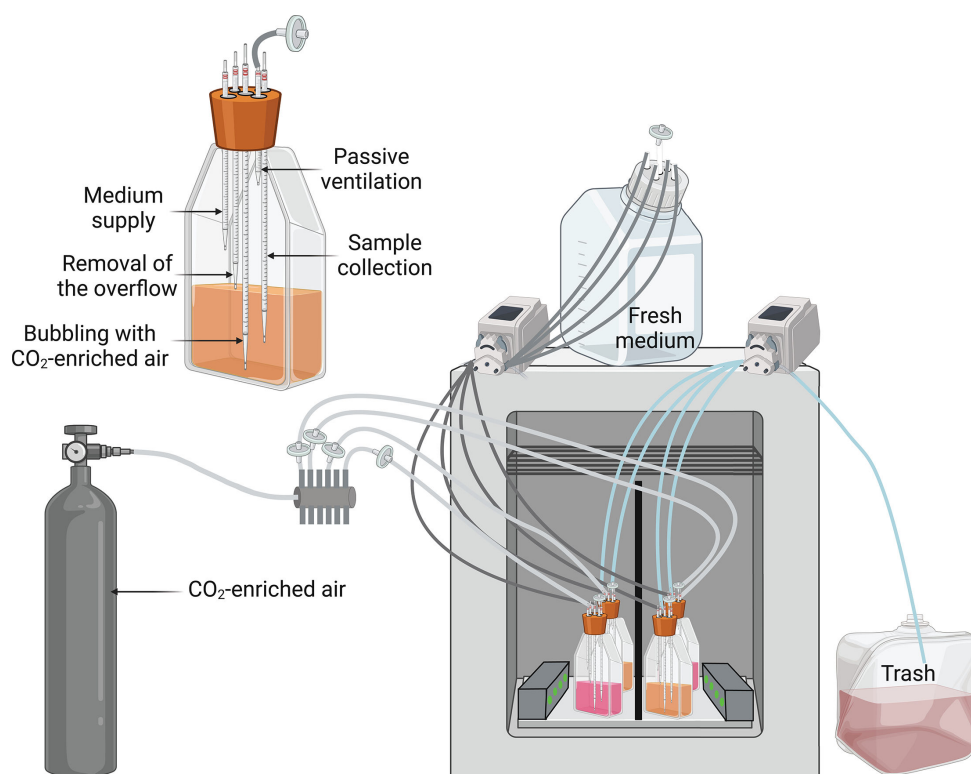


FIG 1 Experimental setup for continuous monocultures and co-cultures in chemostats. The insert in the top left corner is a zoom on one of the flasks shown in the general view. Note that the complete setup consisted of three growth cabinets, with one light condition per cabinet, allowing one to run 12 continuous cultures at the same time. Only one cabinet is shown here for readability.

Fluorimetry

Photosystem II quantum yield

Measurements of the PSII quantum yield (F_V/F_M), a proxy for the maximum photosynthetic activity of the cells, were carried out three times per week after 5 min acclimation to dark using a multi-wavelength fluorometer Phyto-PAM II (Walz), as previously described (35) except that five wavelengths (440, 480, 540, 590, or 625 nm) of modulated light were used.

PSII cross-section

The PSII cross-section ($\sigma(II)_\lambda$), which represents the PSII functional antenna size (36), was measured twice during the experiments (growth phase and steady state) and only in monocultures. The O-I fluorescence fast kinetics, which refers to the increase of fluorescence yield induced by a strong actinic light, was recorded with a Phyto-PAM II (Walz), as described elsewhere (37). PSII cross-section values were calculated using the Phytowin 3 software (38); at 480 nm (cyan) and 540 nm (green), the two wavelengths closest to PUB ($\lambda_{\max} \approx 495$ nm) and PEB ($\lambda_{\max} \approx 550$ nm) absorption peaks, respectively.

PSII electron transport

Like the PSII cross-section, the linear electron transport rate through PSII (ETR_{II}) was measured twice (during the growth phase and in steady state) in monocultures at 480 and 540 nm. As described in reference 37, the basal fluorescence F_0 was recorded before samples were exposed to 13 steps of increasing light irradiance (90 seconds each). At the end of each step, the instantaneous (F_t) and maximal (F'_M) fluorescence levels were

recorded, allowing the computation of PSII quantum yield under illuminated conditions $\left(\frac{F'_V}{F'_M}\right)$. The ETRII at each step was calculated as follows:

$$\text{ETRII} = \frac{\left(\left(\frac{F'_V}{F'_M}\right) \times \sigma(II)_\lambda \times I \times 0.6022\right)}{\frac{F_V}{F_M}} \quad (\text{Eq. 7})$$

where I represents instantaneous irradiance (38).

Finally, ETRII values for each step were plotted against their corresponding light irradiance. The photosynthesis Platt model (39) was then fitted to these curves and used to compute the PSII efficiency under non-saturating light (α [37]).

Spectrofluorimetry

In vivo fluorescence spectra were recorded several times a week using a FL6500 spectrofluorimeter (Perkin-Elmer) and analyzed with the Fluorescence software (Perkin-Elmer), as described elsewhere (21). Briefly, excitation spectra were acquired between 450 and 560 nm (with emission set at 580 nm) and emission spectra between 550 and 750 nm (with excitation set at 530 nm). The $\text{Exc}_{495:550}$ fluorescence excitation ratio was used as a proxy of the whole cell PUB:PEB ratio. $\text{Em}_{560:650}$ and $\text{Em}_{650:680}$ fluorescence emission ratios were used to estimate the PE to PC as well as the PC to PBS terminal acceptor (TA) ratios, respectively. The PE:PC ratio provided insights into the electron transfer efficiency within the PBS and the length of PBS rods, and the PC:TA ratio into the coupling between the PBS and PSII reaction center chlorophylls.

Real-time quantitative PCR

Design of the probes and optimization

Because it was not possible to differentiate all pigment types by flow cytometry under some conditions, particularly under BL, where the CA4-capable strain and the BL specialist had indistinguishable fluorescence signals, a real-time quantitative PCR approach was developed to assess the relative abundance of each pigment type within the co-cultures. For each strain, primers were designed using Geneious (version 11.0.5). Target genes were selected as being single copy and strain-specific, based on patterns of gene presence/absence in the Cyanorak information system (Table S1 [40]). Each set of primers was tested for specificity and optimized using DNA extracted from cultures of the three studied strains.

Sampling, cell lysis, DNA extraction, and purification

Five milliliter of each co-culture was sampled daily, filtered through 0.2 μm Supor filters of 25 mm diameter (Pall Life Sciences), and stored in 2 mL Eppendorf tubes at -80°C until analysis. DNA was extracted from the 0.2 μm Supor filters following a protocol adapted from previous studies (41, 42). After thawing the filters on ice, 350 μL of lysis buffer (50 mM TRIS, 20 mM EDTA, pH 8.0) and a 5 mm steel bead were added to each Eppendorf. The samples were then ground for 30 s at 30 Hz using a TissueLyser (MM300, Retsch) to break the cell wall at room temperature. To ensure complete cell lysis, filters were incubated with 175 μL lysozyme (50 mg mL^{-1} , Sigma-Aldrich) for 45 min at 37°C under agitation (Thermomixer comfort, Eppendorf). 70 μL of SDS (10%, Invitrogen) and 35 μL of proteinase K (20 mg mL^{-1} , Sigma-Aldrich) were added, and filters were again incubated under agitation for 2.5 h at 55°C . DNA samples were then treated by adding 70 μL of RNase (20 mg mL^{-1} , Sigma-Aldrich) for 10 min at room temperature. The filters and the aqueous phases were immediately transferred to 2 mL Phase Lock GelTM (PLG) tubes (QuantaBio, VWR). To dissolve the filters, increase DNA extraction efficiency and remove protein contaminants, two phenol:chloroform:isoamyl alcohol (25:24:1 vol/vol; Eurobio) and one chloroform:isoamyl alcohol (24:1 vol/vol; Sigma-Aldrich) extractions

were conducted. For each, 700 μL of organic extraction mix was added to the PLG tubes. After mixing, the tubes were subsequently centrifuged for 5 min at $1,500 \times g$ and 18°C using an Eppendorf 5417R centrifuge. The aqueous phase was then recovered and transferred to new PLG tubes. Finally, the DNA in the aqueous phase was purified using silica gel columns (DNeasy Blood and Tissue Kit, Qiagen) following the manufacturer's protocol for Gram-negative bacteria. DNA was eluted in 200 μL nuclease-free water (Invitrogen). 260:280 and 260:230 ratios were measured to assess the DNA purity using an ND-1000 spectrophotometer (Nanodrop).

Preparation of real-time PCR standards from *Synechococcus* cultures

Template DNA was obtained from exponentially growing *Synechococcus* cultures of each strain harvested by centrifugation at 4°C , $14,000 \times g$ for 10 min using an Eppendorf 5804R centrifuge in the presence of 0.01% Pluronic acid (Sigma-Aldrich). 200 μL of ATL buffer (Qiagen) was added to the pellets before grinding using a 5 mm steel bead, as described above. Then, samples were incubated under agitation (Thermomixer comfort, Eppendorf) with 10 μL lysozyme (50 mg mL^{-1} , Sigma-Aldrich) for 45 min at 37°C . After the addition of 200 μL of AL buffer (Qiagen) and 15 μL of proteinase K (20 mg mL^{-1} , Sigma-Aldrich), samples were incubated under agitation for 2.5 h at 55°C . 200 μL ethanol 100% (Sigma-Aldrich) was immediately added to the samples, which were vortexed and purified using silica gel columns (DNeasy Blood and Tissue Kit, Qiagen) following the manufacturer's instructions. DNA was eluted in 100 μL nuclease-free water (Invitrogen). As for the co-culture samples, DNA 260:280 and 260:230 ratios and concentrations were quantified using a ND-1000 spectrophotometer (Nanodrop).

Real-time PCR

Reactions for real-time PCR were prepared by mixing 6 μL of ONEGreen FAST qPCR Premix (Ozyme), 0.12 μL of forward and reverse primers stock (final concentration of 300 $\mu\text{mol L}^{-1}$, Eurogentec), 0.76 μL of nuclease-free water (Invitrogen), and 5 μL of template DNA. Template DNA for the standard curves was serially diluted 10-fold over 7 orders of magnitude to obtain standard concentrations ranging from 50 to $5 \cdot 10^{-6}$ ng per well. Template DNA from the co-culture samples was not diluted. Each reaction was performed in triplicate. Real-time SYBR Green fluorescence data were acquired using a LightCycler 480 (Roche) and the program recommended by the manufacturer. The baseline and threshold cycle (C_T) were estimated automatically with the "Abs Quant/2nd Derivative Max" of the LightCycler 480 software (version 1.5.0, Roche). For co-culture samples, each quantification cycle (C_q) was converted to DNA concentration based on the standard curve equation. The number of target gene copies per well was then estimated using Dhanasekaran et al.'s formula (43) and converted to copies per mL based on the volume of the filtered co-culture, the total amount of DNA extracted, and the amount of template DNA added in each well. Results were expressed as the percentage of each strain in the co-culture at any given time of the experiments.

Comparative genomics

The repertoire of genes involved in the biosynthesis or regulation of PBS components was compared between the three *Synechococcus* strains using the Cyanorak genome database (<https://cyanorak.sb-roscoff.fr/cyanorak/?execution=e2s1> [40]). The number of phycobilin lyases, the enzymes responsible for the covalent binding of chromophores to phycobiliproteins, encoded in each genome was then used to predict the chromophorylation of each α - β heterodimer based on the extensive literature on lyase function (see <https://cyanolyase.genouest.org/>), while the PBS linker content was used to estimate the PBS rod length (15).

Biovolume

For each tested light condition, the biovolume of each strain (Table S2) was estimated at steady state using an Eclipse 80i fluorescence microscope equipped with a Cy3 filter (Nikon). Photographs were taken at 100× magnification using a SPOT RT3 camera (Diagnostic Instruments Inc.) under GL excitation ($\lambda_{\text{max}} = 550 \text{ nm}$) to observe their natural orange fluorescence. Analysis of the photographs was done with SPOT Advanced software (Diagnostic Instruments Inc.) to measure the length (L) and width (W) of 100–150 cells. The biovolume (V) was calculated assuming that *Synechococcus* cells have a short-rod shape, using the following formula:

$$V = (L - W) \times \pi \times \left(\frac{W}{2}\right)^2 + \left[\frac{4}{3} \times \pi \times \left(\frac{W}{2}\right)^3\right] \quad (\text{Eq. 8})$$

Dissolved nutrient analyses

Phosphate (PO_4^{3-}), nitrate (NO_3^-), and ammonium (NH_4^+) concentrations were quantified in steady state following standardized protocols (44, 45).

Statistics

Statistical analyses were carried out using the R software (version 4.2.3; R Core Team, 2021 [46]) to compare the pigment and photosynthetic characteristics of (i) a given strain in the different light conditions tested (LBL, LGL, HBL, and HGL) and (ii) the three different strains in a given light condition. One-way ANOVA or Kruskal-Wallis (stats package version 3.6.2) tests were performed, after checking for the normality (Shapiro-Wilk's test; stats package version 3.6.2) and variance homogeneity (Levene's test; car package version 3.1-3) of the data, and followed by Tukey's (stats package version 3.6.2) or Dunn's post hoc tests (dunn.test package version 1.3.6), respectively. The same approach was used to compare critical light intensities, that is, irradiances transmitted through the cultures at steady state (47, 48), for each PT representative and each specific light condition.

Estimation of model parameters

All model parameters were estimated from monoculture experiments. System parameters such as the incident intensities of LBL and LGL ($I_{\text{in,LBL}}$ and $I_{\text{in,LGL}}$), the depth of the chemostat vessel z_m , and the dilution rate D were defined by the experimental settings (Table 2). We assumed that the specific loss rates of the strains were determined by the dilution rate of the chemostat vessel (i.e., $m_i = D$). Light absorption coefficients (k_i) of the three *Synechococcus* strains and background turbidity (K_{bg}) were estimated for each combination of light color and light intensity (i.e., LBL, LGL, HBL, and HGL). First, based on equation 1, for each monoculture, we plotted the values of $\ln(I_{\text{out},j}/I_{\text{in},j})/z_{\text{max}}$ versus C_i measured at each time point of the experiment. Linear regression analysis was then applied, and the light absorption coefficient (k_i) and background turbidity (K_{bg}) were estimated as the slope and intercept of the linear regression. Finally, the estimates of K_{bg} and k_i obtained from these regression analyses were averaged over the replicates of each treatment. The photosynthetic efficiencies (ϕ_i) of the three *Synechococcus* strains were estimated for each light condition by fitting the time courses of population density (C_i) and light transmitted through the chemostats (I_{out}) predicted by the model to the time courses observed in the monoculture experiments, using a least-squares method (48).

The parameter estimates obtained from the monoculture experiments are summarized in Table 2. These monoculture estimates were used to predict the time courses and outcomes of the competition experiments.

TABLE 2 Model parameters estimated from the monoculture experiments^a

Symbol	Definition	Value			Units
Variables					
C_i	Biomass of phytoplankton species i	$-^e$			$\text{mm}^3 \text{L}^{-1}$
$I_{\text{out}}(\text{BL})$	BL transmitted through chemostats	$-$			$\mu\text{mol photons m}^{-2} \text{s}^{-1}$
$I_{\text{out}}(\text{GL})$	GL transmitted through chemostats	$-$			$\mu\text{mol photons m}^{-2} \text{s}^{-1}$
System parameters					
$I_{\text{in}}(\text{BL})$	Incident BL intensity	15			$\mu\text{mol photons m}^{-2} \text{s}^{-1}$
$I_{\text{in}}(\text{GL})$	Incident GL intensity	15			$\mu\text{mol photons m}^{-2} \text{s}^{-1}$
$K_{\text{bg}}(\text{BL})$	Mean background turbidity for BL	9.80			m^{-1}
$K_{\text{bg}}(\text{GL})$	Mean background turbidity for GL	8.17			m^{-1}
z_{max}	Maximum depth of the water column	0.05			m
D	Dilution rate ^b	0.1			d^{-1}
Species parameters		<i>BL specialist</i>	<i>GL specialist</i>	<i>CA4-capable</i>	
$\phi_i(\text{BL})$	Photosynthetic efficiency in BL	0.900×10^{-3}	n.d. ^c	0.480×10^{-3}	$\text{mm}^3 \mu\text{mol}^{-1}$
$\phi_i(\text{GL})$	Photosynthetic efficiency in GL	1.700×10^{-3}	1.840×10^{-3}	1.060×10^{-3}	$\text{mm}^3 \mu\text{mol}^{-1}$
$k_i(\text{BL})$	Specific light absorption coefficient in BL	0.272	n.d. ^c	0.148	$\text{m}^2 \text{mm}^3$
$k_i(\text{GL})$	Specific light absorption coefficient in GL	0.113	0.130	0.131	$\text{m}^2 \text{mm}^3$
	Cell volume ^d	0.846	1.22	1.15	$\mu\text{m}^3 \text{cell}^{-1}$
Critical light intensities		<i>BL specialist</i>	<i>GL specialist</i>	<i>CA4-capable</i>	
$I_{\text{out}}(\text{BL})$	Critical light intensity in LBL	2.53	n.d. ^c	5.73	$\mu\text{mol photons m}^{-2} \text{s}^{-1}$
$I_{\text{out}}(\text{GL})$	Critical light intensity in LGL	7.58	1.70	6.93	$\mu\text{mol photons m}^{-2} \text{s}^{-1}$

^aAbbreviations: BL, blue light; GL, green light; LBL, low blue light; LGL, low green light.

^bWe assume that specific loss rates of the species are dominated by the dilution rate of the chemostat (i.e., $m_i = D$).

^cn.d.: no data; the GL specialist did not grow well in LBL, and hence we could not determine its species parameters in BL.

^dPredicted population densities in $\text{mm}^3 \text{L}^{-1}$ were converted with the cell volume to obtain population densities in cells L^{-1} .

^e– indicates that the value is not unique but varies with strains and conditions.

RESULTS

Monocultures

Time course of cell densities and light penetration in different light conditions

To better understand how each of the three main *Synechococcus* PTs thriving in the open ocean (26) individually behave in different conditions of light quantity and quality, we first performed continuous monocultures of one representative strain for each PT: RS9902, a BL specialist (PT 3c); RS9907, a GL specialist (PT 3a); and RS9915, a CA4-capable strain (PT 3dB; Table 1).

During the experiments, the cell density gradually increased to a steady state (Fig. 2A, D and Fig. 3A, D), causing a gradual decrease in the intensity of light transmitted through the culture flasks (I_{out} ; Fig. 2B, E and Fig. 3B, E). Two parameters derived from these measurements, namely the cell concentration at steady state and the critical light intensity (I_{out}), that is, the light intensity transmitted through the culture at steady state (47, 48), were used to fit the model. The PSII quantum yield (F_V/F_M), a proxy of the maximum photosynthetic activity of the cells, was also measured on a regular basis during the experiment to gain insights about the physiological status of the cells (Fig. 2C, F and Fig. 3C, F).

In LBL, the BL specialist grew faster than the CA4-capable strain and reached steady state with cell densities of $\approx 3.6 \times 10^7$ cells mL^{-1} by approximately the 35th day of monitoring (Fig. 2A). In comparison, the CA4-capable strain stabilized more than 12 days later at similar or slightly higher cell concentrations ($\approx 3.9 \times 10^7$ cells mL^{-1} for one replicate and $\approx 6.4 \times 10^7$ cells mL^{-1} for the other). Despite several attempts ($n = 5$), the GL

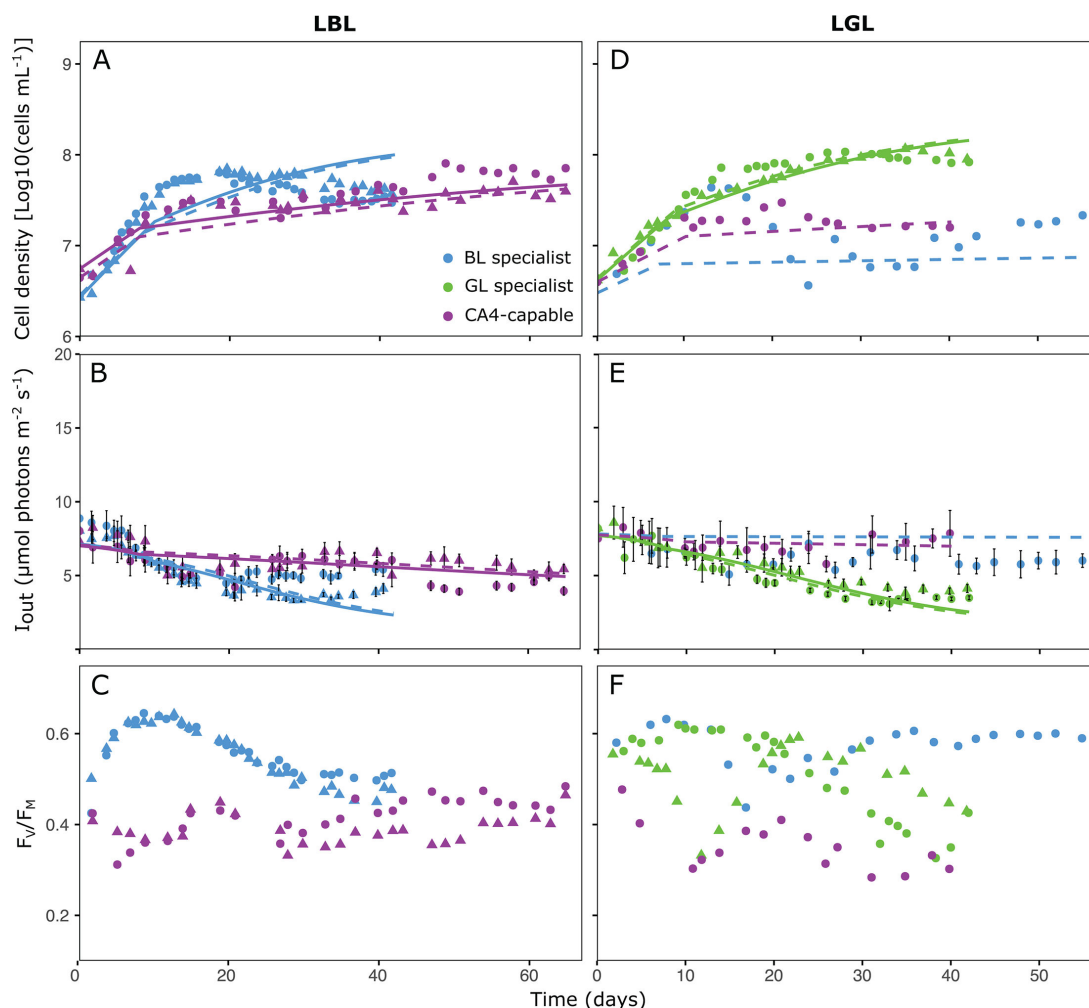


FIG 2 Monocultures of three marine *Synechococcus* strains representative of different pigment types in low blue and green light conditions. (A through C) Low blue light (LBL). (D through F) Low green light (LGL). (A and D) Cell density. (B and E) Light transmitted through the culture flasks (I_{out}). (C and F) Photosystem II quantum yield (F_V/F_M). Error bars in panels B and E correspond to the average and standard deviation of five different measurements on the side of the flask opposite to the light source. Shapes indicate different replicates (circles for replicate A and triangles for replicate B). Dashed (for replicate A) and solid (for replicate B) lines represent the input of the model. Note that each data point series within a graph corresponds to an independent monoculture (i.e., a single strain), and that the time needed for cells to reach the steady state, and thus the duration of the experiment, may vary between strains and light conditions.

specialist was not able to grow in LBL, likely because its growth rate in this light condition was lower than the dilution rate. The I_{out} was statistically similar for the BL specialist and the CA4-capable strain (4.46 ± 0.99 and 4.85 ± 0.85 $\mu\text{mol photons m}^{-2} \text{s}^{-1}$, respectively; one-way ANOVA, P -value > 0.05 ; Fig. 2B and Table S3). However, the CA4-capable strain exhibited a lower F_V/F_M than its counterpart throughout the experiments (Fig. 2C).

In contrast to LBL, the GL specialist grew well in LGL and reached high cell concentrations in steady state ($\approx 1.2 \times 10^8$ cells mL^{-1} ; Fig. 2D). Conversely, the growth of the two other strains was most likely limited by light. In our single successful attempt (out of 5) to grow them in this light condition, the BL specialist and CA4-capable strain stabilized at much lower cell densities ($\approx 1.9 \times 10^7$ and $\approx 1.6 \times 10^7$ cells mL^{-1} , respectively) than the GL specialist. Consistently, the GL specialist also reached the lowest I_{out} (3.70 ± 0.47 $\mu\text{mol photons m}^{-2} \text{s}^{-1}$, as compared to 5.92 ± 0.12 and 7.61 ± 0.26 $\mu\text{mol photons m}^{-2} \text{s}^{-1}$ for the BL specialist and CA4-capable strain, respectively; one-way ANOVA, P -value < 0.05 ; Fig. 2E and Table S3). As in LBL, the CA4-capable strain exhibited the lowest F_V/F_M of all

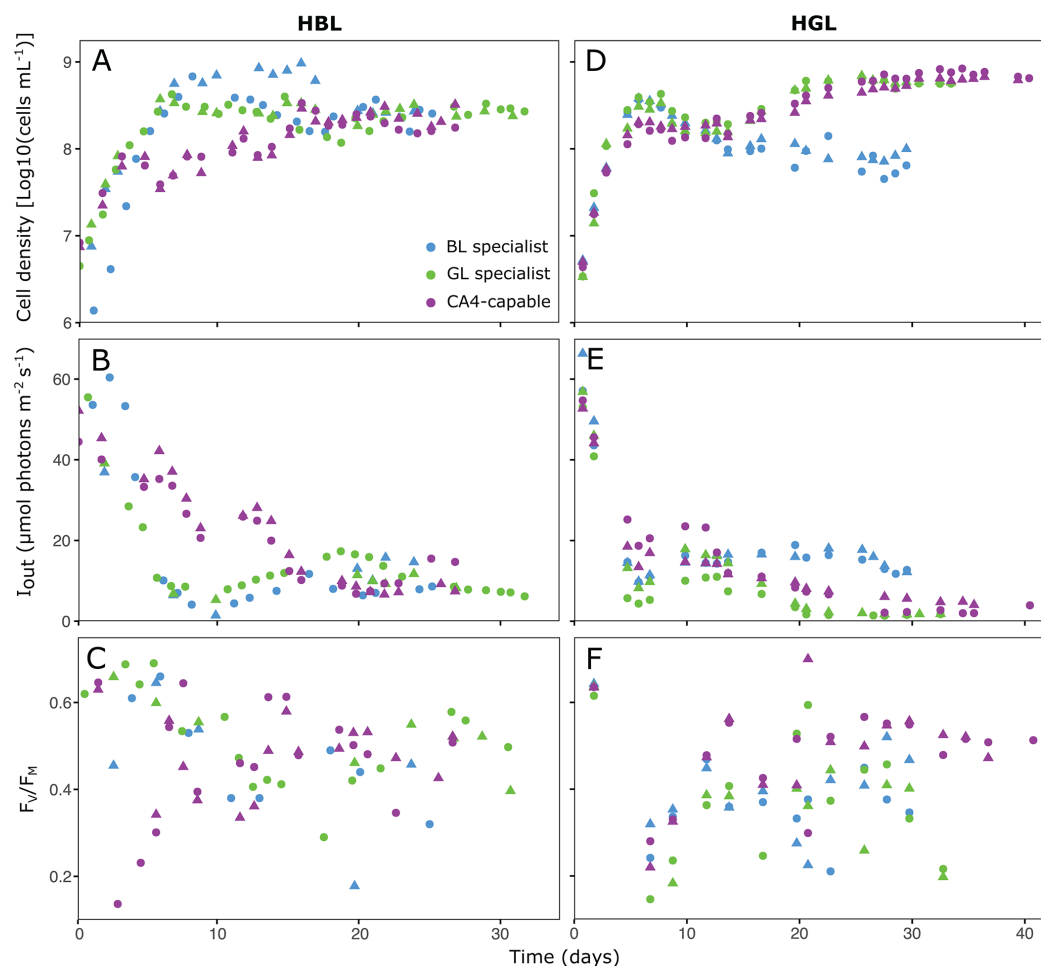


FIG 3 Same as Fig. 2 but in high blue light (HBL; A–C) and high green light (HGL; D–F) conditions.

strains in LGL (Fig. 2F), suggesting that its photosynthesis was less efficient in LL compared to both specialists.

In both LBL and LGL, the model was in most cases able to correctly capture the dynamics of population density and I_{out} , and in particular for the CA4-capable strain.

In HBL, the BL and GL specialists grew faster than the CA4-capable strain, both reaching their highest cell concentrations ($\approx 9.6 \times 10^8$ and 4.3×10^8 cells mL⁻¹, respectively) during the first 2 weeks of the experiments (Fig. 3A). However, the three PTs stabilized at similar cellular densities in steady state ($\approx 2.2 \times 10^8$ cells mL⁻¹) and had statistically similar I_{out} (10.43 ± 4.17 for the BL specialist, 8.60 ± 1.65 for the GL specialist, and 10.08 ± 3.04 μmol photons m⁻² s⁻¹ for the CA4-capable strain; Kruskal-Wallis, P -value > 0.05 ; Fig. 3B and Table S3).

In HGL, although all three PTs grew at similar rates at the beginning of the experiments, only the GL specialist and the CA4-capable strain achieved maximum cell concentrations of $\approx 6.3 \times 10^8$ cells mL⁻¹ at steady state (Fig. 3D). In this light condition, the GL specialist reached the lowest I_{out} (1.66 ± 0.22 μmol photons m⁻² s⁻¹, compared to 14.76 ± 2.25 and 3.84 ± 1.73 μmol photons m⁻² s⁻¹ for the BL specialist and the CA4-capable strain, respectively; Kruskal-Wallis, P -value < 0.05 ; Fig. 3E and Table S3). In contrast to LL, all strains exhibited a strong variability of F_v/F_m over the course of the experiments in HL, without any clear pattern, even though CA4-capable cells clearly reached higher values than at LL (Fig. 3C and F). One possible explanation for this

variability could be that their growth rate was much faster in HL than LL, creating some fluctuations in pH levels, which we might have overseen since the pH was controlled only once per day. Transient alkalization was indeed previously reported in the diatom *Thalassiosira pseudonana* to cause a drop of F_V/F_M , but not in growth rate (49).

In HL conditions, the model was only able to capture the initial increase in population density, but with an overestimation of the steady-state population density (Fig. S2A), or to capture the steady-state population density, but with an underestimation of the initial increase in population density (Fig. S2B). These poor fits of the population dynamics caused similarly poor fits of the dynamics in I_{out} and this applied to almost all strains in both HBL and HGL. Hence, the model could not adequately describe the HL experiments in monoculture, and therefore was not applied to the HL competition experiments in co-culture.

Comparison of pigment and photosynthetic characteristics between the different strains

To better characterize the pigment and photosynthetic properties of each strain, and therefore better explain their distinct growth behaviors, additional measurements were performed on monocultures in the different tested light conditions.

The ratio of whole-cell fluorescence excitation at 495 and 550 nm ($Exc_{495:550}$), a proxy of the PUB:PEB ratio of the cells, remained constant during the experiments and did not differ between light conditions for both the BL specialist (1.58 ± 0.04) and the GL specialist (0.39 ± 0.01), as expected from their fixed pigmentation (Fig. 4A). Also as expected from Humily et al. (10), the CA4-capable strain displayed a low $Exc_{495:550}$ ratio in HGL (0.72 ± 0.07) and high $Exc_{495:550}$ ratios in LBL (1.69 ± 0.06) and HBL (1.52 ± 0.07). Surprisingly, however, the $Exc_{495:550}$ ratio of the CA4-capable strain increased during the time course of LGL monocultures, from a minimal value of 0.7 at the beginning of the experiment to an intermediate value of 1.03 ± 0.11 at steady state (Fig. 4; Fig. S3). This suggests that the CA4-capable strain perceived a change in the light spectrum as the monocultures became denser, and accordingly adjusted its PUB:PEB ratio to optimize energy collection.

To better interpret observed differences in PUB:PEB ratios between the strains, comparative analyses of their phycobilisome gene content, and more particularly of their phycobilin lyase gene content (Table S4), were made to predict the chromophorylation of phycobiliproteins at each cysteine binding site (Table S5), and thus to assess the molar PUB:PEB ratio per phycobilisome in both BL and GL (Table S6). These analyses predicted that the BL specialist and the BL-acclimated CA4-capable strain should exhibit the same molar PUB:PEB ratio (1.18), in agreement with their similar $Exc_{495:550}$ ratio in LBL and HBL (Fig. 4A and S1). This implies that the different growth behaviors of the BL specialist and the CA4-capable strain recorded in LBL and HBL (Fig. 2A and 3A) cannot be explained by a difference in PUB:PEB ratio. By contrast, the molar PUB:PEB ratio of the GL specialist (0.22) is predicted to be almost twice as low as that of the CA4-capable strain (0.39) in GL, in agreement with the observed difference in $Exc_{495:550}$ ratio between these strains (Fig. 4; Fig. S1).

The ratio of whole-cell fluorescence emission at 560 and 650 nm ($Em_{560:650}$), a proxy for the phycoerythrin to phycocyanin (PE:PC) ratio of the cells, was systematically higher for the BL specialist than for the GL specialist, even though both exhibited some slight but statistically significant variations of their ratios depending on light conditions (Fig. 4B). Interestingly, the CA4-capable strain exhibited $Em_{560:650}$ ratios similar to the BL specialist in both LL conditions and to the GL specialist in HL conditions. By comparison, the ratio of whole-cell fluorescence emission at 650 nm and 680 nm ($Em_{650:680}$), a proxy of the PC to terminal acceptor (PC:TA) ratio of the cells, varied little between light treatments for all three strains, although it was generally lower for the GL specialist than for the two other strains (Fig. S4).

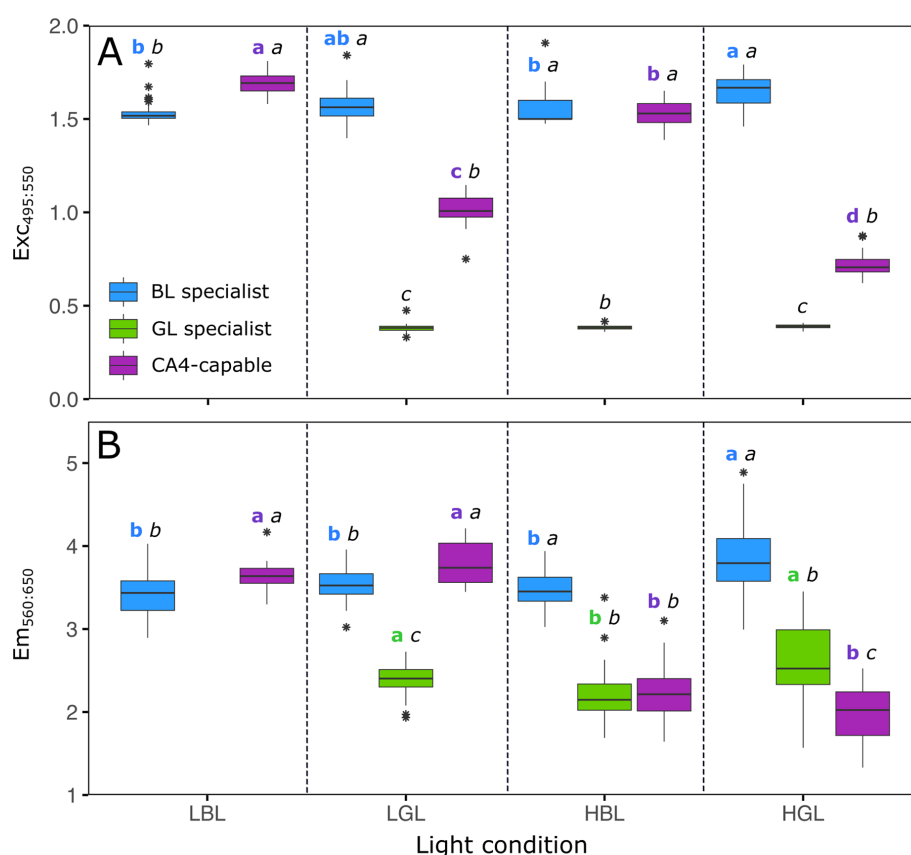


FIG 4 Mean $\text{Exc}_{495:550}$ fluorescence excitation ratio and $\text{Em}_{560:650}$ fluorescence emission ratio for the three *Synechococcus* strains grown in monocultures in the different light conditions used in this study. (A) $\text{Exc}_{495:550}$ fluorescence excitation ratio, a proxy for the whole-cell PUB:PEB ratio. (B) $\text{Em}_{560:650}$ fluorescence emission ratio, a proxy for the whole-cell PE:PC ratio. Box plots represent all measurements performed every 2 days over the course of the experiments. The different letters above boxplots indicate statistical test results (one-way ANOVA followed by Tukey's test, or Kruskal-Wallis followed by Dunn's test). The first bold-colored letter compares the values displayed by a given strain in the four different light conditions tested. The second italic black letter compares the values exhibited by the three different strains in a given light condition.

As expected from the respective color preference of each PT, the PSII cross-section [$\sigma(II)_{\lambda}$] as well as the PSII efficiency under non-saturating light (α) were both generally higher at 480 nm (cyan) than 540 nm (green) for the BL specialist, and conversely for the GL specialist (Fig. S5 and S6). The GL specialist was characterized by the highest σ and α values of all three strains at 540 nm in all light conditions where this strain grew, while the BL specialist exhibited the highest σ and α values at 480 nm in high light conditions only (Fig. S5 and S6). The CA4-capable strain displayed either low or intermediate σ values at both wavelengths, suggesting that its antenna size was smaller than specialists in their preferred color (Fig. S5). In addition, it generally had α values similar to (or even smaller than) specialists in their non-preferred color, suggesting that it had a fairly weak PSII efficiency under non-saturating irradiances (Fig. S6). A notable exception is the LBL condition, in which the CA4-capable strain exhibited higher σ and α values than the BL specialist at 480 nm.

Competition experiments

Competition theory predicts that, if several species compete for a single color of light, then the species with the lowest critical light intensity (I_{out}) for this color will be the superior competitor (31, 47, 48). Hence, the I_{out} values estimated from the monoculture

experiments can be used to predict the winners of a competition for light. The I_{out} of the LL monocultures was estimated in two different ways: directly from the measurements of I_{out} in monoculture at steady state (Table S3), and indirectly from the steady-state value of I_{out} predicted by the model using the parameter estimates obtained from the LL monocultures (Table 2). Since the model could not adequately capture the population dynamics of the monocultures in HL, the I_{out} in these conditions was estimated only from the measurements of I_{out} in monocultures. This resulted in the following predictions.

(i) In LBL, the measured I_{out} of the BL specialist and the CA4-capable strain were within the same range (Table S3), but the model analysis indicated that the I_{out} was lower for the BL specialist than for the CA4-capable strain (Table 2). Hence, the model predicted that the BL specialist should win.

(ii) In LGL, the measurements and the model analysis both showed that the I_{out} was lowest for the GL specialist (Table 2; Table S3). Hence, the GL specialist was predicted to win.

(iii) In HBL, the measured I_{out} did not differ significantly between the three strains (Table S3), and hence were too close to reliably predict which of these three strains should be the best competitor in this light condition.

(iv) In HGL, the GL specialist had the lowest measured I_{out} (Table S3), and hence was predicted to win the competition.

To test these predictions, continuous co-cultures were established with the three pigment type representatives in the same light conditions as for the monocultures. In LL, each of the BL and GL specialists won the competition in their favorite light color (Fig. 5A and B), while the abundance of the other PTs decreased. Therefore, the model was able to accurately predict the population dynamics during the competition experiments in both LL treatments (Fig. 5A and B).

Although the temporal dynamics of the different strains in co-cultures was more variable between the two biological replicates in HL than LL treatments, the prediction proved valid for the HGL condition, where the BL specialist and the CA4-capable strain were completely outcompeted by the GL specialist at steady state (Fig. 5D). In HBL, where the model was unable to predict the outcome of competition, the co-culture experiment interestingly showed that the CA4-capable strain represented 85%–90% of the total *Synechococcus* population at the end of the monitoring (Fig. 5C), the remainder being shared by the two specialists.

Nutrients

Quantification of NH_4^+ , NO_3^- , and PO_4^{3-} in steady state demonstrated that none of the mono- and co-cultures were nutrient-limited in LL (Table S7). The HGL cultures had the highest steady-state cell densities, and hence the observation that these cultures had the lowest steady-state nutrient concentrations is in line with expectation. Furthermore, very sharp drops of NH_4^+ concentration were observed in both HGL and HBL cultures, with a majority of measurements below $50 \mu\text{mol L}^{-1}$ and a minimum value of $13 \mu\text{mol L}^{-1}$. As a consequence, all three strains mainly assimilated nitrogen in the form of NO_3^- (50), as indicated by the decrease in the NO_3^- stock over the course of the experiments. However, NO_3^- was sufficiently abundant at steady state in all cultures (above $900 \mu\text{mol L}^{-1}$) for the strains not to be nitrogen-limited. The concentration of PO_4^{3-} also decreased in HL over the course of the experiments (minimum: $20 \mu\text{mol L}^{-1}$). However, it has been reported that marine *Synechococcus* strains grown in chemostats are able to grow at near maximum rates at PO_4^{3-} concentrations below 10 nM (51). The conditions used by these authors, being quite similar to ours (continuous culture, 24°C , $35 \mu\text{mol photons m}^{-2} \text{s}^{-1}$, 12 h light-dark cycles), it is unlikely that our cultures faced phosphorus deficiency. These nutrient measurements demonstrate that, like for LL cultures, HL cultures were neither nitrogen- nor phosphorus-limited.

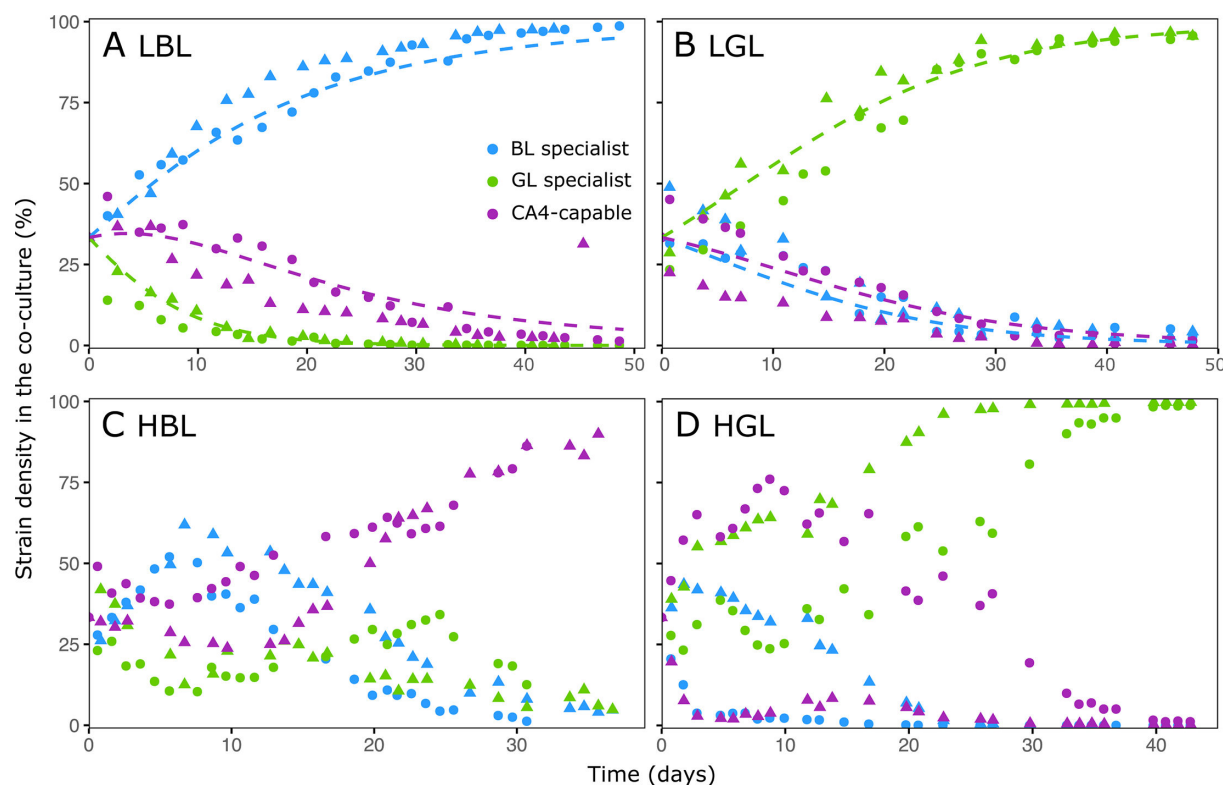


FIG 5 Time course changes in co-cultures of the relative cell density of the three marine *Synechococcus* strains in the four tested light conditions, as determined by a combination of qPCR and flow cytometry approaches. (A) Low blue light (LBL). (B) Low green light (LGL). (C) High blue light (HBL). (D) High green light (HGL). Shapes indicate different replicates (circles for replicate A and triangles for replicate B). Dashed lines in panels A and B represent the input of the model.

DISCUSSION

While CA4-capable cells globally constitute the major *Synechococcus* PT in wide expanses of the world's Ocean (26), the reasons for their ecological success are as yet unclear. One of the main current hypotheses, first evoked to explain the fitness advantage of a cyanobacterium exhibiting CA3 over either a red light specialist (PT 1) or a green-yellow light specialist (PT 2 [6, 52]), is that cells capable of chromatic acclimation would be better suited than specialists to sustain growth in a fluctuating underwater light field (53). Using a mathematical model of the ocean column, the authors of the latter study found that deeper mixed layers selected for CA4-capable strains in simulated mixtures of *Synechococcus* PTs. However, results from their model did not match the actual distribution of PTs in the ocean, since they found no correlation between the relative abundance of CA4-capable strains and mixed layer depths, consistent with previous work (26). Alternatively, CA4-capable strains could perform better than specialists in certain light conditions. To test this hypothesis, we (i) performed continuous monocultures of a BL specialist, a GL specialist, and a CA4-capable strain in different conditions of light quantity and quality; (ii) predicted the outcomes of competition experiments for light with a resource competition model; and (iii) verified the theoretical predictions by co-culturing strains representative of all three PTs.

Results of co-culture experiments in LGL and HGL were consistent with competition theory, which predicted that the strain with the lowest I_{out} should be the superior competitor and thus displace its counterparts (47, 48). In both light conditions, the GL specialist displayed the lowest I_{out} (Fig. 2E and 3E; Table S3) and was the only remaining strain at steady state in the co-cultures (Fig. 5B and 5D). This result was expected since the GL specialist was by far the best suited of the three PTs to harvest green photons. The GL specialist indeed not only possesses PBS with a much lower molar PUB:PEB ratio (0.22) than the other two strains (0.39 for the CA4-capable strain acclimated to GL, and

1.18 for the BL specialist; Table S6), but also has by far the largest photosynthetic antenna size (Fig. S5B) and PSII efficiency under non-saturating light (Fig. S6B) of all three PTs at 540 nm.

The outcome of co-culture experiments in LBL also matched the model predictions since the BL specialist outcompeted the CA4-capable strain. This result might seem surprising since the latter strain exhibited a significantly larger antenna size (Fig. S5A) and PSII efficiency under non-saturating light (Fig. S6A) at 480 nm than the BL specialist. Yet, the CA4-capable strain also displayed a much lower PSII quantum yield (F_V/F_M) than its counterpart all over the course of the experiment (Fig. 2C), indicating that its photo-physiological status was suboptimal in LBL. This may partly explain why the CA4-capable strain was almost completely excluded by the BL specialist in the LBL co-culture (Fig. 5A). Regarding our inability to grow the GL specialist in LBL, our hypothesis is that the ambient photon flux in this light condition was too low to sufficiently feed its photosynthetic light reactions given the limited overlap between the wavelength range emitted by the blue LEDs and the fluorescence excitation spectrum of the GL specialist (Fig. S1A). This caused a rapid population loss due to continuous dilution ($D = 0.1 \text{ day}^{-1}$) that likely exceeded its growth rate. Such a scenario was previously evoked to describe the competition for light between two microalgae (28).

The outcome of co-culture experiments in HBL was more complex to interpret since the BL specialist and CA4-capable strain displayed very similar I_{out} (Table S3), making it difficult to predict the best competitor based on these parameters. Photo-physiological measurements of monocultures revealed some interesting differences between the two PTs. On the one hand, the larger photosynthetic antenna size (Fig. S5A) and PSII efficiency under non-saturating light (Fig. S6A) of the BL specialist could *a priori* have conferred it a competitive advantage over the CA4-capable strain in HBL. On the other hand, the almost two times higher $\text{Em}_{560:650}$ ratio of the BL specialist compared to the CA4-capable strain in this light condition (Fig. 4B) might reflect a lower energy transfer efficiency within PBS rods for the former strain, and thus explains the lower competitiveness of the BL specialist observed in this light condition. Given this uncertainty, the possibility that other factors are involved in the observed superiority of the CA4-capable strain in HBL cannot be ruled out, though allelopathy can likely be excluded since we checked for the absence of microcin-C biosynthesis genes in both genomes (54). It is also worth noting that the high residual nitrate and phosphate concentrations (above 900 and 20 $\mu\text{mol L}^{-1}$, respectively) indicate that nitrogen and phosphorus did not limit the growth of the HL cultures. However, it is possible that the availability of some other elements (e.g., trace metals) became limiting or co-limiting in the very dense HL cultures, which may have affected competitive interactions between the strains. Overall, future studies using different sets of specialists and CA4-capable strains isolated from different geographical locations and grown under a larger range of experimental conditions, including mixes of BL and GL, would be needed. In particular, these studies could test whether the faster growth of the CA4 strain in HBL compared to the BL specialist may not result from differences in nutrient uptake strategies. In addition, it would be interesting to check whether a PT 3dA strain in competition with specialists would behave similarly to the PT 3dB strain used in the present study, given their different evolutionary histories (24, 25).

Our results may have important implications for predicting the spectral niches of *Synechococcus* PTs in the world Ocean (5). Indeed, they imply that GL specialists should predominate in greenish environments, independent of depth. Conversely, BL specialists should predominate in blue open ocean waters at depth, where the light intensity is low, while CA4-capable strains would prevail in the upper mixed layer. The first hypothesis is indeed consistent with observations made along the *Tara* Oceans transect by Grébert and co-workers (26), since GL specialists were found to predominate at all depths in green waters in ocean margin areas. Yet, these authors also reported a globally higher relative abundance of BL specialists in surface than at depth, while the reverse was true for chromatic acclimators. This global trend might, however, translate to different local

situations since, in temperate areas, surface and deep *Synechococcus* populations often belong to different lineages that may exhibit different PTs (11, 26).

This study also brought some novel insights concerning the perception of light quality by CA4-capable cells. Indeed, the variations of the PUB:PEB ratio observed over the course of the experiment in some light conditions, notably in LGL (Fig. S1 and S3), suggests that the CA4-capable strain perceived and quickly responded to a gradual change in the light quality occurring within the flask as the culture became denser, even though there was no change in ambient light color in the incubator. Interestingly, our results also revealed the previously unknown capacity of a CA4-capable strain to adjust its PE:PC ratio depending on light intensity (Fig. 4B), a behavior previously described in a CA3-capable strain but in response to a change in light color (6). When grown in white light with either a red light or a GL specialist, the CA3-capable strain was indeed found to modify its PE:PC ratio to harvest the part of the light spectrum not used by its competitor, while keeping the total amount of these two pigments constant. In the present case, a possible explanation for the observed decrease in the PE:PC ratio of the CA4-capable strain with light intensity is that it may enable a modulation of energy transfer efficiency along the PBS rods.

Conclusions

Previous studies predicted that flexible phenotypes would often be weaker competitors than specialists in mono-color conditions (52, 55). Although we confirmed that specialists were the winners at LL in their favorite light color, and that the GL specialist was the best competitor in HGL, we also found that the CA4-capable strain was actually able to outcompete the other PTs in HBL.

Overall, our results demonstrated that both the light quality and quantity had major effects on the outcome of co-culture experiments. Still, given the interplay between competition for the underwater light field and other important selective factors, such as nutrients or temperature, more studies are needed to better understand the spatio-temporal variability of the distribution of the different *Synechococcus* PTs at the global scale and refine predictions of global models (5, 56).

ACKNOWLEDGMENTS

We thank members of the CRBM (Centre de Recherche en Biologie Marine, Roscoff) for sharing the temperature-controlled room and CO₂ system used in this study, as well as Sarah Bureau for taking care of nutrient analyses. We are also most grateful to Christophe Six and Sarah Garric for technical hints on PAM fluorimetry, as well as Priscillia Gourvil, Martin Gachenot, and Michele Grego from the Roscoff Culture Collection for providing *Synechococcus* strains.

AUTHOR AFFILIATIONS

¹Sorbonne Université, CNRS, UMR 7144 Adaptation and Diversity in the Marine Environment (AD2M), Ecology of Marine Plankton (ECOMAP) team, Station Biologique de Roscoff (SBR), Roscoff, France

²Sorbonne Université, CNRS, UMR 7093 Laboratoire d'Océanographie de Villefranche (LOV), Institut de la Mer de Villefranche (IMEV), Villefranche-sur-Mer, France







³Department of Biology, Indiana University, Bloomington, Indiana, USA

⁴Department of Freshwater and Marine Ecology (FAME), Institute for Biodiversity and Ecosystem Dynamics, University of Amsterdam, Amsterdam, the Netherlands

PRESENT ADDRESS

Louison Dufour, Institute of Microbiology, CAS Centre Algatech, Třebon, Czechia

AUTHOR ORCID*s*

Louison Dufour  <http://orcid.org/0009-0006-6938-2547>
 Laurence Garczarek  <https://orcid.org/0000-0002-8191-8395>
 Morgane Ratin  <http://orcid.org/0000-0002-1696-2322>
 David M. Kehoe  <http://orcid.org/0000-0003-2675-8576>
 Jef Huisman  <http://orcid.org/0000-0001-9598-3211>
 Jolanda M. H. Verspagen  <http://orcid.org/0000-0001-9295-4183>
 Frédéric Partensky  <http://orcid.org/0000-0003-1274-4050>

FUNDING

Funder	Grant(s)	Author(s)
Agence Nationale de la Recherche	ANR-19-CE02-0019	Laurence Garczarek Francesco Mattei Frédéric Partensky
National Science Foundation	MCB-1029414	David M. Kehoe
National Science Foundation	MCB-1818187	David M. Kehoe

AUTHOR CONTRIBUTIONS

Louison Dufour, Conceptualization, Data curation, Formal analysis, Investigation, Methodology, Validation, Visualization, Writing – original draft, Writing – review and editing | Laurence Garczarek, Conceptualization, Funding acquisition, Project administration, Supervision, Writing – original draft, Writing – review and editing | Francesco Mattei, Methodology, Validation, Writing – review and editing | Bastian Gouriou, Investigation, Methodology, Validation | Julia Clairet, Investigation, Methodology, Validation | Morgane Ratin, Investigation, Methodology, Validation | David M. Kehoe, Validation, Writing – review and editing | Jef Huisman, Methodology, Validation, Writing – review and editing | Jolanda M. H. Verspagen, Methodology, Validation, Writing – review and editing | Frédéric Partensky, Conceptualization, Formal analysis, Funding acquisition, Project administration, Supervision, Writing – original draft, Writing – review and editing

ADDITIONAL FILES

The following material is available [online](#).

Supplemental Material

Supplemental figures (AEM00087-25-s0001.pdf). Figures S1 to S7.
Supplemental tables (AEM00087-25-s0002.xlsx). Tables S1 to S7.

REFERENCES

- Field CB, Behrenfeld MJ, Randerson JT, Falkowski P. 1998. Primary production of the biosphere: integrating terrestrial and oceanic components. *Science* 281:237–240. <https://doi.org/10.1126/science.281.5374.237>
- Behrenfeld MJ, O'Malley RT, Siegel DA, McClain CR, Sarmiento JL, Feldman GC, Milligan AJ, Falkowski PG, Letelier RM, Boss ES. 2006. Climate-driven trends in contemporary ocean productivity. *Nature* 444:752–755. <https://doi.org/10.1038/nature05317>
- Kirk JTO. 1994. Light and photosynthesis in aquatic ecosystems. 2nd ed. Cambridge University Press.
- Stomp M, Huisman J, Stal LJ, Matthijs HCP. 2007. Colorful niches of phototrophic microorganisms shaped by vibrations of the water molecule. *ISME J* 1:271–282. <https://doi.org/10.1038/ismej.2007.59>
- Holtrop T, Huisman J, Stomp M, Biersteker L, Aerts J, Grébert T, Partensky F, Garczarek L, van der Woerd HJ. 2021. Vibrational modes of water predict spectral niches for photosynthesis in lakes and oceans. *Nat Ecol Evol* 5:55–66. <https://doi.org/10.1038/s41559-020-01330-x>
- Stomp M, Huisman J, De Jongh F, Veraart AJ, Gerla D, Rijkeboer M, Ibelings BW, Wollenzien UIA, Stal LJ. 2004. Adaptive divergence in pigment composition promotes phytoplankton biodiversity. *Nature* 432:104–107. <https://doi.org/10.1038/nature03044>
- Striebel M, Behl S, Diehl S, Stibor H. 2009. Spectral niche complementarity and carbon dynamics in pelagic ecosystems. *Am Nat* 174:141–147. <https://doi.org/10.1086/599294>
- Flombaum P, Gallegos JL, Gordillo RA, Rincón J, Zabala LL, Jiao N, Karl DM, Li WKW, Lomas MW, Veneziano D, Vera CS, Vrugt JA, Martiny AC. 2013. Present and future global distributions of the marine Cyanobacteria *Prochlorococcus* and *Synechococcus*. *Proc Natl Acad Sci USA* 110:9824–9829. <https://doi.org/10.1073/pnas.1307701110>
- Six C, Thomas J-C, Garczarek L, Ostrowski M, Dufresne A, Blot N, Scanlan DJ, Partensky F. 2007. Diversity and evolution of phycobilisomes in marine *Synechococcus* spp.: a comparative genomics study. *Genome Biol* 8:R259. <https://doi.org/10.1186/gb-2007-8-12-r259>

10. Humily F, Partensky F, Six C, Farrant GK, Ratin M, Marie D, Garczarek L. 2013. A gene island with two possible configurations is involved in chromatic acclimation in marine *Synechococcus*. *PLoS One* 8:e84459. <https://doi.org/10.1371/journal.pone.0084459>
11. Grébert T, Garczarek L, Daubin V, Humily F, Marie D, Ratin M, Devailly A, Farrant GK, Mary I, Mella-Flores D, Tanguy G, Labadie K, Wincker P, Kehoe DM, Partensky F. 2022. Diversity and evolution of pigment types in marine *Synechococcus* cyanobacteria. *Genome Biol Evol* 14:evac035. <https://doi.org/10.1093/gbe/evac035>
12. Glazer AN. 1989. Light guides: directional energy transfer in a photosynthetic antenna. *J Biol Chem* 264:1–4. [https://doi.org/10.1016/S0021-9258\(17\)31212-7](https://doi.org/10.1016/S0021-9258(17)31212-7)
13. Ong LJ, Glazer AN. 1991. Phycoerythrins of marine unicellular cyanobacteria. I. Bilin types and locations and energy transfer pathways in *Synechococcus* spp. *phycoerythrins*. *J Biol Chem* 266:9515–9527. [https://doi.org/10.1016/S0021-9258\(18\)92851-6](https://doi.org/10.1016/S0021-9258(18)92851-6)
14. Sidler WA. 1994. Phycobilisome and phycobiliprotein structures, p 139–216. In Bryant DA (ed), *The Molecular Biology of Cyanobacteria*. Springer Netherlands, Dordrecht.
15. Six C, Thomas J-C, Thion L, Lemoine Y, Zal F, Partensky F. 2005. Two novel phycoerythrin-associated linker proteins in the marine cyanobacterium *Synechococcus* sp. strain WH8102. *J Bacteriol* 187:1685–1694. <https://doi.org/10.1128/JB.187.5.1685-1694.2005>
16. Scheer H, Zhao K-H. 2008. Biliprotein maturation: the chromophore attachment: biliprotein chromophore attachment. *Mol Microbiol* 68:263–276. <https://doi.org/10.1111/j.1365-2958.2008.06160.x>
17. Sanfilippo JE, Nguyen AA, Karty JA, Shukla A, Schluchter WM, Garczarek L, Partensky F, Kehoe DM. 2016. Self-regulating genomic island encoding tandem regulators confers chromatic acclimation to marine *Synechococcus*. *Proc Natl Acad Sci USA* 113:6077–6082. <https://doi.org/10.1073/pnas.1600625113>
18. Palenik B. 2001. Chromatic adaptation in marine *Synechococcus* strains. *Appl Environ Microbiol* 67:991–994. <https://doi.org/10.1128/AEM.67.2.991-994.2001>
19. Everrood C, Six C, Partensky F, Thomas J-C, Holtzendorff J, Wood AM. 2006. Biochemical bases of type IV chromatic adaptation in marine *Synechococcus* spp. *J Bacteriol* 188:3345–3356. <https://doi.org/10.1128/JB.188.9.3345-3356.2006>
20. Shukla A, Biswas A, Blot N, Partensky F, Karty JA, Hammad LA, Garczarek L, Gutu A, Schluchter WM, Kehoe DM. 2012. Phycoerythrin-specific bilin lyase-isomerase controls blue-green chromatic acclimation in marine *Synechococcus*. *Proc Natl Acad Sci USA* 109:20136–20141. <https://doi.org/10.1073/pnas.1211777109>
21. Dufour L, Garczarek L, Gouriou B, Clairet J, Ratin M, Partensky F. 2024. Differential acclimation kinetics of the two forms of type IV chromatic acclimators occurring in marine *Synechococcus* cyanobacteria. *Front Microbiol* 15:1349322. <https://doi.org/10.3389/fmicb.2024.1349322>
22. Sanfilippo JE, Garczarek L, Partensky F, Kehoe DM. 2019. Chromatic acclimation in cyanobacteria: a diverse and widespread process for optimizing photosynthesis. *Annu Rev Microbiol* 73:407–433. <https://doi.org/10.1146/annurev-micro-020518-115738>
23. Sanfilippo JE, Nguyen AA, Garczarek L, Karty JA, Pokhrel S, Strnat JA, Partensky F, Schluchter WM, Kehoe DM. 2019. Interplay between differentially expressed enzymes contributes to light color acclimation in marine *Synechococcus*. *Proc Natl Acad Sci USA* 116:6457–6462. <https://doi.org/10.1073/pnas.1810491116>
24. Grébert T, Nguyen AA, Pokhrel S, Joseph KL, Ratin M, Dufour L, Chen B, Haney AM, Karty JA, Trinidad JC, Garczarek L, Schluchter WM, Kehoe DM, Partensky F. 2021. Molecular bases of an alternative dual-enzyme system for light color acclimation of marine *Synechococcus* cyanobacteria. *Proc Natl Acad Sci USA* 118:e2019715118. <https://doi.org/10.1073/pnas.2019715118>
25. Kehoe DM, Biswas A, Chen B, Dufour L, Grébert T, Haney AM, Joseph KL, Kumarapperuma I, Nguyen AA, Ratin M, Sanfilippo JE, Shukla A, Garczarek L, Yang X, Schluchter WM, Partensky F. 2025. Light color regulation of photosynthetic antennae biogenesis in marine phytoplankton. *Plant Cell Physiol* 66:168–180. <https://doi.org/10.1093/pcp/pcae115>
26. Grébert T, Doré H, Partensky F, Farrant GK, Boss ES, Picheral M, Guidi L, Pesant S, Scanlan DJ, Wincker P, Acinas SG, Kehoe DM, Garczarek L. 2018. Light color acclimation is a key process in the global ocean distribution of *Synechococcus* cyanobacteria. *Proc Natl Acad Sci USA* 115:E2010–E2019. <https://doi.org/10.1073/pnas.1717069115>
27. Stomp M, Huisman J, Vörös L, Pick FR, Laamanen M, Haverkamp T, Stal LJ. 2007. Colourful coexistence of red and green picocyanobacteria in lakes and seas. *Ecol Lett* 10:290–298. <https://doi.org/10.1111/j.1461-0248.2007.01026.x>
28. Huisman J, Matthijs HCP, Visser PM, Balke H, Sigon CAM, Passarge J, Weissing FJ, Mur LR. 2002. Principles of the light-limited chemostat: theory and ecological applications. *Antonie Van Leeuwenhoek* 81:117–133. <https://doi.org/10.1023/A:1020537928216>
29. Fuller NJ, Marie D, Partensky F, Vulot D, Post AF, Scanlan DJ. 2003. Clade-specific 16S ribosomal DNA oligonucleotides reveal the predominance of a single marine *Synechococcus* clade throughout a stratified water column in the Red Sea. *Appl Environ Microbiol* 69:2430–2443. <https://doi.org/10.1128/AEM.69.5.2430-2443.2003>
30. Mazard S, Ostrowski M, Partensky F, Scanlan DJ. 2012. Multi-locus sequence analysis, taxonomic resolution and biogeography of marine *Synechococcus*. *Environ Microbiol* 14:372–386. <https://doi.org/10.1111/j.1462-2920.2011.02514.x>
31. Luimstra VM, Verspagen JMH, Xu T, Schuurmans JM, Huisman J. 2020. Changes in water color shift competition between phytoplankton species with contrasting light-harvesting strategies. *Ecology* 101:e02951. <https://doi.org/10.1002/ecy.2951>
32. Rippka R, Coursin T, Hess W, Lichtlé C, Scanlan DJ, Palinska KA, Iteman I, Partensky F, Houmard J, Herdman M. 2000. *Prochlorococcus marinus* Chisholm et al. 1992 subsp. *pastoris* subsp. nov. strain PCC 9511, the first axenic chlorophyll a_2/b_2 -containing cyanobacterium (Oxyphotobacteria). *Int J Syst Evol Microbiol* 50:1833–1847. <https://doi.org/10.1099/0020-7713-50-5-1833>
33. Burson A, Stomp M, Greenwell E, Grosse J, Huisman J. 2018. Competition for nutrients and light: testing advances in resource competition with a natural phytoplankton community. *Ecology* 99:1108–1118. <https://doi.org/10.1002/ecy.2187>
34. Marie D, Partensky F, Vulot D, Brussaard C. 1999. Enumeration of phytoplankton, bacteria, and viruses in marine samples. *CP Cytometry* 10:11. <https://doi.org/10.1002/0471142956.cy1111s10>
35. Pittera J, Humily F, Thorel M, Grulois D, Garczarek L, Six C. 2014. Connecting thermal physiology and latitudinal niche partitioning in marine *Synechococcus*. *ISME J* 8:1221–1236. <https://doi.org/10.1038/ismej.2013.228>
36. Campbell DA, Tyystjärvi E. 2012. Parameterization of photosystem II photoinactivation and repair. *Biochim Biophys Acta Bioenerg* 1817:258–265. <https://doi.org/10.1016/j.bbabi.2011.04.010>
37. Six C, Ratin M, Marie D, Corre E. 2021. Marine *Synechococcus* picocyanobacteria: light utilization across latitudes. *Proc Natl Acad Sci USA* 118:e2111300118. <https://doi.org/10.1073/pnas.2111300118>
38. Schreiber U, Klughammer C, Kolbowski J. 2012. Assessment of wavelength-dependent parameters of photosynthetic electron transport with a new type of multi-color PAM chlorophyll fluorometer. *Photosynth Res* 113:127–144. <https://doi.org/10.1007/s1120-012-9758-1>
39. Platt T, Gallegos CL. 1980. Modelling primary production, p 339–362. In Falkowski PG (ed), *Primary Productivity in the Sea*. Springer US, Boston, MA.
40. Garczarek L, Guyot U, Doré H, Farrant GK, Hoebeke M, Brillet-Guéguen L, Bisch A, Ferrieux M, Siltanen J, Corre E, Le Corguillé G, Ratin M, Pitt FD, Ostrowski M, Conan M, Siegel A, Labadie K, Aury J-M, Wincker P, Scanlan DJ, Partensky F. 2021. Cyanorak v2.1: a scalable information system dedicated to the visualization and expert curation of marine and brackish picocyanobacteria genomes. *Nucl Acids Res* 49:D667–D676. <https://doi.org/10.1093/nar/gkaa958>
41. Tai V, Palenik B. 2009. Temporal variation of *Synechococcus* clades at a coastal Pacific Ocean monitoring site. *ISME J* 3:903–915. <https://doi.org/10.1038/ismej.2009.35>
42. Gutiérrez-Rodríguez A, Slack G, Daniels EF, Selph KE, Palenik B, Landry MR. 2014. Fine spatial structure of genetically distinct picocyanobacterial populations across environmental gradients in the Costa Rica Dome. *Limnol Oceanogr* 59:705–723. <https://doi.org/10.4319/lo.2014.59.3.0705>
43. Dhanasekaran S, Doherty TM, Kenneth J. 2010. Comparison of different standards for real-time PCR-based absolute quantification. *J Immunol Meth* 354:34–39. <https://doi.org/10.1016/j.jim.2010.01.004>
44. Aminot A, Kérouel R. 2007. Dosage automatique des nutriments dans les eaux marines: méthodes en flux continu. Editions Quae, Paris, France.
45. Oriol L, Garcia N, Cariou T, Ferreira S, Jolly O. 2023. Dosage de l'azote ammoniacal en milieu marin par fluorimétrie: protocole national.

- SOMLIT. <https://www.somlit.fr/wpcontent/uploads/2023/01/09-Protocol-e-ammonium-fluorimetrie-2023.pdf>.
46. R Core Team. 2021. R: A language and environment for statistical computing. Vienna, Austria R foundation for Statistical Computing. <https://www.R-project.org/>.
 47. Huisman J, Weissing FJ. 1994. Light - limited growth and competition for light in well - mixed aquatic environments: an elementary model. *Ecology* 75:507–520. <https://doi.org/10.2307/1939554>
 48. Huisman J, Jonker RR, Zonneveld C, Weissing FJ. 1999. Competition for light between phytoplankton species: experimental tests of mechanistic theory. *Ecology* 80:211–222. [https://doi.org/10.1890/0012-9658\(1999\)080\[0211:CFLBPS\]2.0.CO;2](https://doi.org/10.1890/0012-9658(1999)080[0211:CFLBPS]2.0.CO;2)
 49. Oberlander JL, Burke ME, London CA, MacIntyre HL. 2025. Assessing the impacts of simulated ocean alkalinity enhancement on viability and growth of nearshore species of phytoplankton. *Biogeosciences* 22:499–512. <https://doi.org/10.5194/bg-22-499-2025>
 50. Berube PM, Rasmussen A, Braakman R, Stepanauskas R, Chisholm SW. 2019. Emergence of trait variability through the lens of nitrogen assimilation in *Prochlorococcus* *Elife* 8:e41043. <https://doi.org/10.7554/eLife.41043>
 51. Kretz CB, Bell DW, Lomas DA, Lomas MW, Martiny AC. 2015. Influence of growth rate on the physiological response of marine *Synechococcus* to phosphate limitation. *Front Microbiol* 6:85. <https://doi.org/10.3389/fmicb.2015.00085>
 52. Stomp M, van Dijk MA, van Overzee HMJ, Wortel MT, Sigon CAM, Egas M, Hoogveld H, Gons HJ, Huisman J. 2008. The timescale of phenotypic plasticity and its impact on competition in fluctuating environments. *Am Nat* 172:E169–E185. <https://doi.org/10.1086/591680>
 53. Lovindeer R, Ustick LJ, Primeau F, Martiny AC, Mackey KRM. 2021. Modeling ocean color niche selection by *Synechococcus* blue - green acclimators . *JGR Oceans* 126:e2021JC017434. <https://doi.org/10.1029/2021JC017434>
 54. Paz-Yepes J, Brahamsha B, Palenik B. 2013. Role of a microcin-C-like biosynthetic gene cluster in allelopathic interactions in marine *Synechococcus*. *Proc Natl Acad Sci USA* 110:12030–12035. <https://doi.org/10.1073/pnas.1306260110>
 55. Lovindeer R, Abbott L, Medina H, Mackey KRM. 2021. Costs and limitations of marine *Synechococcus* blue-green chromatic acclimation. *Front Mar Sci* 8:689998. <https://doi.org/10.3389/fmars.2021.689998>
 56. Mattei F, Hickman AE, Uitz J, Dufour L, Vellucci V, Garczarek L, Partensky F, Dutkiewicz S. 2025. Chromatic acclimation shapes phytoplankton biogeography. *Sci Adv* 11:eadr9609. <https://doi.org/10.1126/sciadv.adr9609>